

RESEARCH

Open Access



Discrimination of healthy oral tissue from oral cancer based on the mean grey value determined by optical coherence tomography

Kangwei Zhou^{1,2†}, Kaili Zheng^{3†}, Li Huang^{1,2†}, Xianglong Zheng^{1,2}, Canyang Jiang^{1,2}, Jianping Huang^{1,2}, Rihui Wang^{1,2}, Xin Ruan^{1,2}, Weicai Jiang^{1,2}, Wen Li^{1,2}, Qingliang Zhao^{3*} and Lisong Lin^{1,2*}

Abstract

Objective This study aimed to identify a quantitative index for optical coherence tomography (OCT) images to discriminate tumours from surrounding tissues.

Subjects and methods Based on OCT measurements, mean grey values were determined from 432 locations on fifty-four human tissue specimens (eighteen cancerous, para-cancerous, and normal tissues each). These results were histologically evaluated by hematoxylin and eosin staining (H&E).

Results The mean grey values of oral squamous cell carcinoma (OSCC) measurements were significantly different from those of the surrounding healthy tissue (p value < 0.0001), with the former being higher. The sensitivity and specificity of detecting tumourous tissue using this approach were 93 and 94%, respectively.

Conclusions OCT as a non-invasive, real-time imaging method, correlates well with H&E pathological images. It can effectively distinguish squamous cell carcinoma from normal tissues with high sensitivity and specificity and is thus expected to assist and guide tumour margin evaluation.

Clinical relevance This discovery highlights the potential of OCT in the objective evaluation of tumour margin during surgery.

Keywords Oral squamous cell carcinoma, Discrimination, Mean grey value, Optical coherence tomography

[†]Kangwei Zhou, Kaili Zheng and Li Huang contributed equally to this work.

*Correspondence:
Qingliang Zhao
drzhaoqingliang@yeah.net
Lisong Lin
drlinls@yeah.net

¹Department of Oral and Maxillofacial Surgery, The First Affiliated Hospital of Fujian Medical University, Fuzhou, China

²Department of Oral and Maxillofacial Surgery, Binhai Campus of the First Affiliated Hospital, National Regional Medical Center, Fujian Medical University, Fuzhou, China

³State Key Laboratory of Molecular Vaccinology and Molecular Diagnostics, Organ Transplantation Institute Center for Molecular Imaging and Translational Medicine, School of Public Health, Xiamen University, Xiamen, China



Introduction

Oral squamous cell carcinoma (OSCC) is a peculiar kind of cancer that develops in the tissues of the mouth, tongue, and lips and has been generally recognised as one of the most common malignancies worldwide [1]. At present, surgical resection of the tumour is the primary therapeutic efficacy of OSCC, while complete resection is the primary aim.

However, complete resection remains challenging, with low success rates of positive resection margins rates at 30 to 40% and local recurrence rates at 25 to 50% [2]. As a result of the low success in complete resection and other factors, the 5-year survival rate for patients diagnosed with OSCC remains less than 50% [3, 4].

Currently, surgeons rely heavily on inspection and palpation as intraoperative approaches to distinguish tumorous tissue from healthy tissue, causing high tumour-positive resection margins. Therefore, a frozen section (FS) assessment plays a mainstay role in evaluating resection margins intraoperatively [5–7]. However, as FS only detects specific sites of the tumour resection margins, it is also prone to sampling error, occasionally generating false negative results [2, 8, 9]. These setbacks create the urgent need to seek a novel tool that supports surgeons in the intraoperative assessment of margins in removed tumour samples.

Multiple techniques for surgical tumour differentiation have been explored to date, such as ultrasound [10], impression cytology [11], and various optical-based techniques [12–15]. Some of these techniques have been applied for OSCC, and recently reviewed by Kain et al. [6]. Optical techniques, such as fluorescent dyes [16], Raman spectroscopy [17], autofluorescence imaging [18], narrow band imaging [19], and optical coherence tomography [20], are promising tools due to their simplicity of operation, relatively lower cost, fast imaging speed, and comprehensiveness.

Optical coherence tomography (OCT) is a well-established, non-invasive optical imaging technology that can image biological samples with high speed and high resolution. It has been applied in the clinical examination of ophthalmology-related conditions [21–23]. OCT's imaging principle mainly depends on refraction and light scattering in the tissue. OCT is able to distinguish different spectral and structural characteristics between cancerous and normal tissues [24]. Similarly, OCT has been used for the early diagnosis and intraoperative discrimination of OSCC [5, 20, 25]. The current diagnosis or peri-operative differentiation of OSCC by OCT is dominantly based on comparing OCT images and histopathological images. However, OCT have not been translated into clinical application. The reason maybe is the lack of quantitative analysis and unified diagnostic criteria. Thus, Mean Grey Value (MGV) may be a useful tool.

MGV is a conventional quantitative index in medical imaging [26–28]. Grey value is deemed as brightness or the depth of colour in the black-and-white images, ranging from 0 to 255, where 0 is black, and 255 is white. During imaging, the contrast of the red (R), green (G), and blue (B) channels is extracted and converted to a grey-scale image. Previously, differences in MGV were found between tumours and normal tissues, such as the thyroid and breast. However, these studies were conducted using ultrasound and CT approaches [32, 33]. The application of MGV in OCT has been scarcely reported, and the utilization of MGV-assisted OCT for differentiating oral cancer from normal tissue is even less common.

The OCT imaging technique offers a rapid acquisition rate, which, in conjunction with MGV, renders it highly suitable for real-time applications. In this research, OCT images of excised tissues after OSCC surgery were quantified and assessed for feasibility in discriminating tumours from surrounding (normal) tissues using the MGV of OCT images.

Materials and methods

Tissue samples

Fifty-four human tissue specimens, consisting of eighteen cancerous, para-cancerous, and normal tissues each were excised from eighteen patients undergoing surgery for OSCC of the tongue and examined. Specimen collection was part of the standard therapeutic surgery protocol performed at the first affiliated Hospital of the Fujian Medical University. Experimental procedures were reviewed by the Ethics Committee of the Fujian Medical University, with patients' privacy protected and conducted in line with human ethics.

OCT system and image acquisition

Experiments were carried out on a home-built SD-OCT system as shown in Fig. 1. The principle and physics of the system are similar to those described in previous studies [29–31]. The light source of this SD-OCT system consisted of a superluminescent diode with a centre wavelength of 840 nm and a bandwidth of 45 nm. The interference signal was collimated and detected by a spectrometer, which consisted of a diffraction grating or prism (1200-line/mm grating and 2048 line), a beam expander, a convergence mirror, and a CCD camera (2048 pixels with 14 μm pixel size, e2V). The calibrated axial resolutions, lateral resolutions, and maximum imaging depth of the system were 5 μm , 15 μm , and 3 mm in air, respectively. The output power was 5 mW, while other details are described in our previous work [30].

The oral tissues were placed in a photosensitive polymer 3D-printed groove module to reduce micromotion effects. Next, the samples were fixed on an X-Y-Z adjusting platform to facilitate adjustment during imaging. The

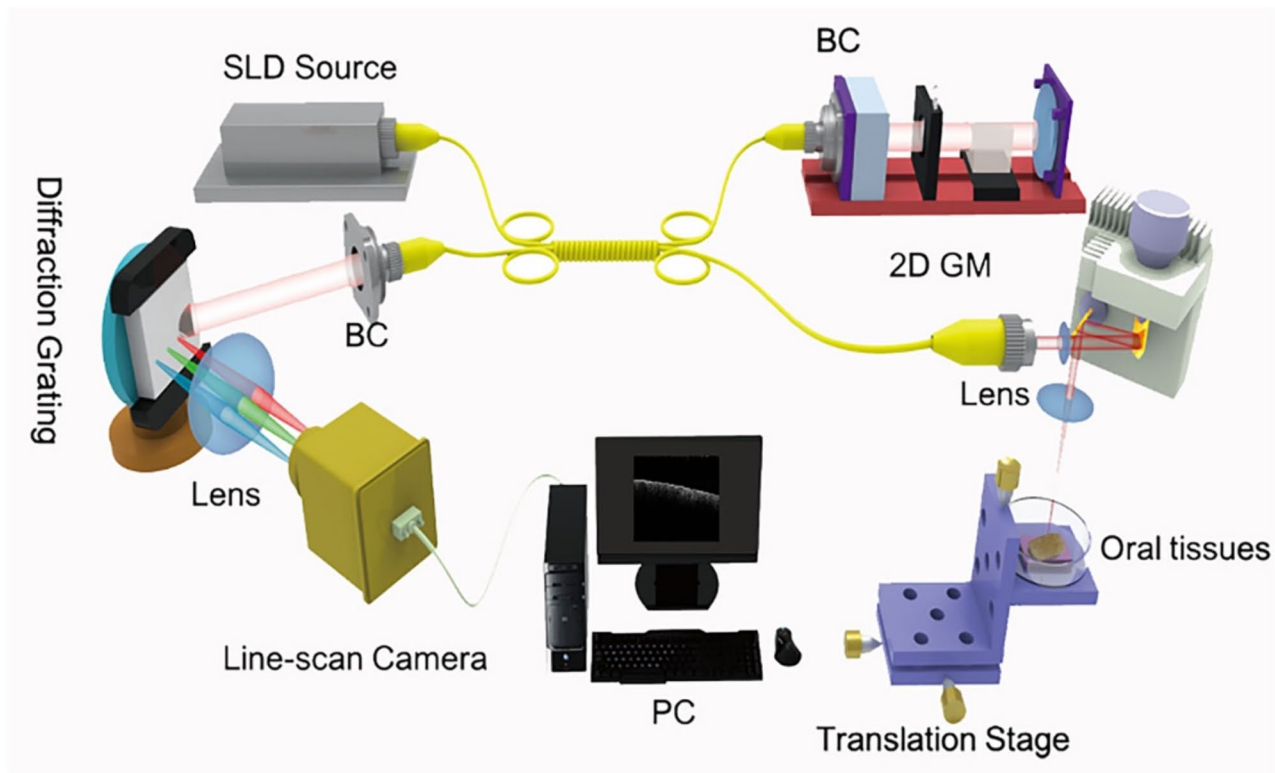


Fig. 1 Schematic diagram of the experimental setup. All oral tissues were investigated using this home-built SD-OCT system. SLD: Superluminescent Diode; BC: Beam Collimator; GM: Galvo Mirrors; PC: Personal Computer

sample arm was adjusted to focus the beam on the tissues. The samples were positioned to ensure optimal signal-to-noise ratio and well-contrasted 2-D images.

Measurement protocol

Three experimental groups were included in the study, with eighteen tissues in each group (cancerous, para-cancerous, and normal tissues). Each tissue was scanned and three OCT images were taken. Before imaging para-cancerous tissue samples, a tiny needle was inserted at the tumour boundary for demarcation (shown in Fig. 2B). Two oral and maxillofacial surgeons determined the tumour boundary, mainly by tissue texture, colour, and shape. Compared with normal tissue, the tumour's texture was firm, with white colouration.

Before OCT imaging, we would place the specimen on a foam plate and mark the imaging locations firstly. OCT images were obtained from the marked locations. After the OCT measurements, the specimen was placed in formalin and processed for routine clinical histopathological evaluation as well as histopathological assessment of each of the locations marked for OCT measurements. These assessments were used for definitive histopathological annotation of the measured locations. (Figs. 2C and 2D). The Image J software was then used to measure the MGV of the images. Each OCT image of the

tumour and normal tissues was measured three times, at selected areas of $0.5 \text{ mm} \times 0.1 \text{ mm}$, and each OCT image of the para-cancerous tissue was measured twice, once on the left and right sides of the marker (Fig. 2A, E and F). All MGVs were tested separately by two researchers. The intra-class correlation coefficient (ICC) was used to assess the consistency of MGV measurements between two researchers. The size of the regions of interest (ROI) in this experiment was the same ($0.5 \text{ mm} \times 0.1 \text{ mm}$), and efforts were meticulously made to position the ROIs at a consistent depth relative to the superficial layer of the tissue. The ROIs were situated as proximate as feasible to the superficial tissue without containing any dark background atop the tissue's surface.

Data analysis

The Mann-Whitney U test was used to determine the statistical difference in the MGVs between OSCC and normal tissue. The ability to distinguish normal tissue from OSCC was determined using the ROC (Receiver Operating Characteristic) curve. The ROC curve was generated based on the specificity and sensitivity of the MGV, as a marker to distinguish tumours from normal tissue. As a diagnostic marker, the optimal threshold MGV was determined by the Youden index (the highest specificity and sensitivity).

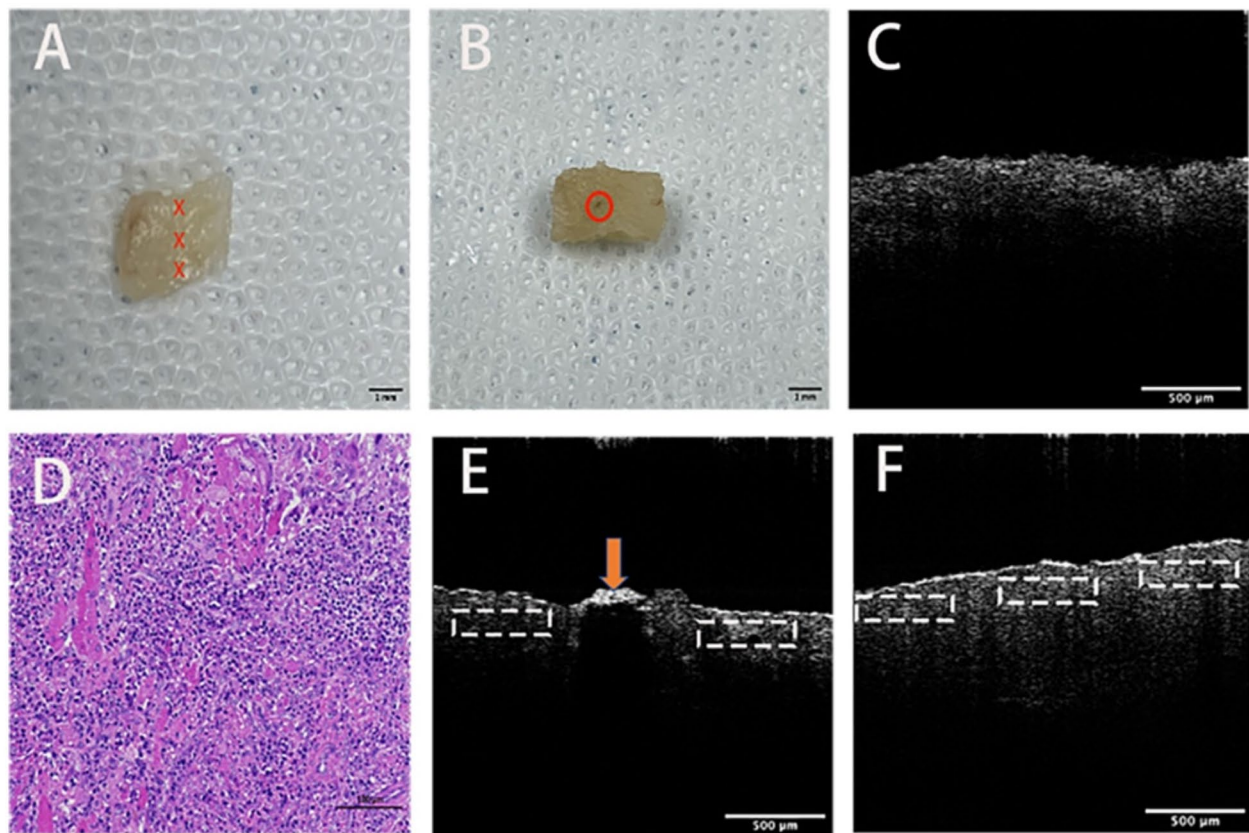


Fig. 2 Overview of measurement protocol. (A) Each tissue was imaged three times, with the imaging position shown with a red x. (B) As shown in the circle, a needle was used to mark the junction areas of the tumour and normal tissues. (C) The obtained OCT image. (D) Specimens were stained with routine hematoxylin and eosin stain after OCT was done. (E) and (F) Using Image J to measure the mean grey values, the white box was the estimated region, and the orange arrow was the needle shown as (B)

Results

A total of 162 OCT and H&E images were analysed, while 432 selected regions were measured and MGVs were obtained. The intra-class correlation coefficient was 0.85 [95% CI: 0.71–0.94], which indicated that the MGV measurement was reliable by different researchers.

OCT findings of the para-cancerous tissue

A significant difference in MGV was found in the OCT images of the para-cancerous tissues, between the two sides of the marked points (Fig. 3A). The surgeon selected the needle's insertion point to obtain OCT pictures of the para-cancerous tissues. In addition, clear MGV boundaries could also be found in the other two OCT images of the same tissue (Fig. 3B and C), confirmed through the corresponding greyscale (Fig. 3D and F) and the MGV curve (Fig. 3G and I). In Fig. 3G and I, the MGV on one side is significantly higher than that of the other, corresponding to OCT images (Fig. 3A and C) and greyscale images (Fig. 3D and F) that were also marked with arrows and dotted lines, whereby G0, H0, and I0 represented low

signal value and G1, H1, and I1 represented high signal value.

OCT signals in the G1, H1, and I1 regions were significantly higher than that in the surrounding tissues, which was consistent with the results of the MGV curves. Therefore, it was speculated that there was a difference between the MGV in the SCC tissue versus the healthy tissue.

Histology and OCT images analysis

Typical examples of OCT images of SCC and normal tissues are shown in Fig. 4. Normal tissue (Fig. 4A) had apparent gaps that were also seen in the H&E stained tissue section (Fig. 4B and C). On the contrary, SCC's OCT image was tightly structured and had no gaps (Fig. 4D), similar to the H&E stained SCC (Fig. 4E and F).

H&E staining also revealed muscle fibres of normal morphology and structure, regular arrangement, and a large number of tumour cells (black arrow) in between the tissues. Connective tissue hyperplasia was seen around the tumour tissue (red arrow). The H&E section on the routine histopathological examination did not

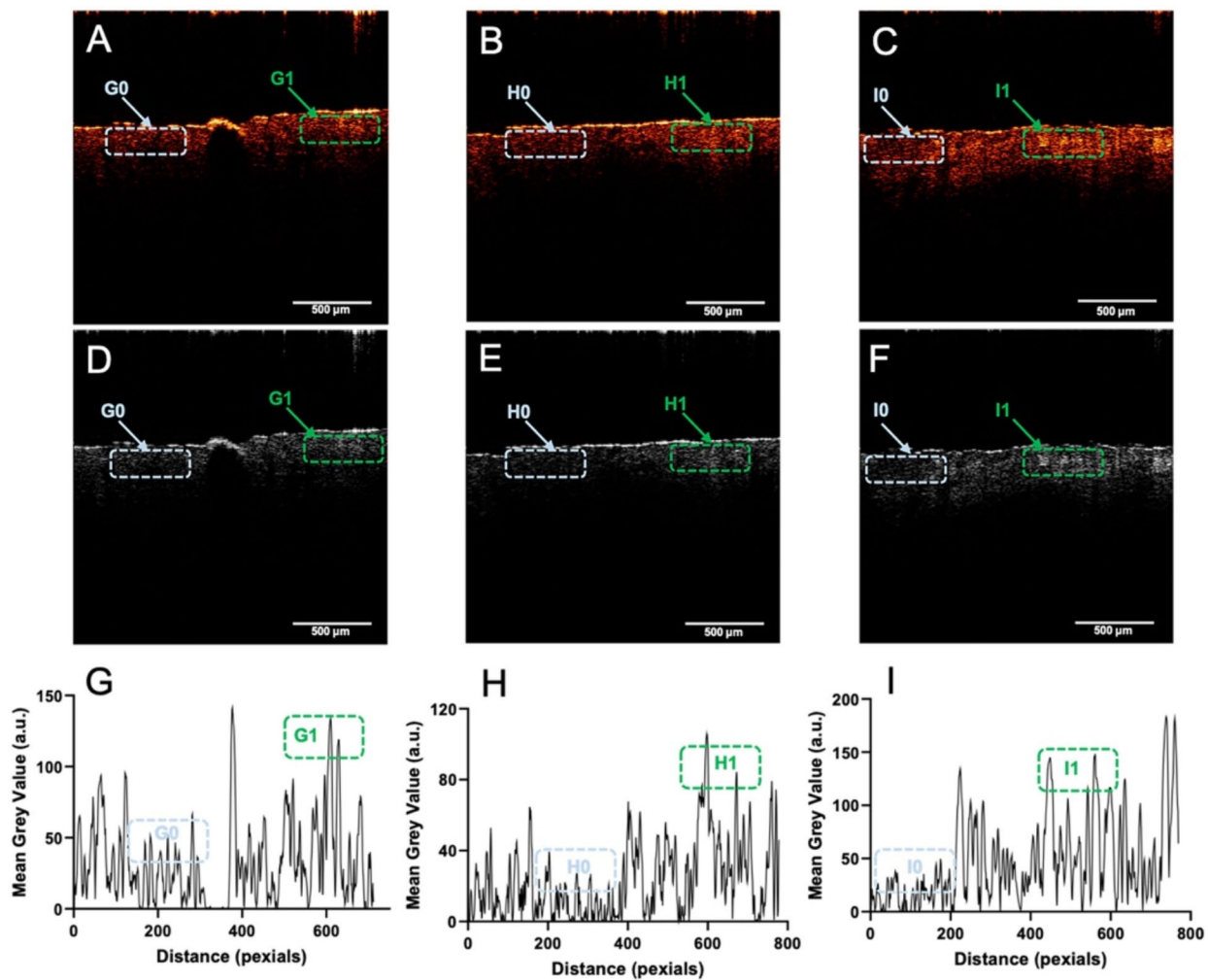


Fig. 3 OCT image finding of the para-cancerous tissues. (A-C) Three OCT images of para-cancerous tissues. (D-F) Greyscale images correspond to A-C images. (G-I) MGv at the a line in Figs. D-F, respectively. The arrows and dashed lines indicated that MGv is significantly higher than the surrounding tissues. And a combination of letters and numbers (G0-I1) was used to distinguish different parts. The presented series of images primarily illustrates the gray values at the line of normal tissues and lesions; however, it is important to note that these images serve exclusively for visual representation and do not constitute the methodology for MGv measurement in the current study

demonstrate degeneration or damage in all measured areas. The OCT experiments also did not interfere with the histological approach.

Statistical significance of mean grey value to differentiate normal tissue and OSCC

After histopathological assessments, half of the MGVs of OCT were marked as SCC and the other half as normal tissue. The normal tissue was mainly muscle.

Figure 5A shows the MGVs of all measured points as evaluated by histopathology. In most cases, the MGv of OSCC was higher than that of normal tissue. The apparent separation of data points showed a significant difference between both groups, which was confirmed by the Mann-Whitney U test. The MGv of OSCC was

significantly higher than that of the surrounding normal tissue, as shown in Fig. 5B ($p < 0.0001$).

A ROC curve was generated based on all measurements to study the use of MGv as a diagnostic marker in tumour resection. The true positive rate (sensitivity) and false positive rate of different MGv thresholds were drawn. The area under the ROC curve was 0.98, as shown in Fig. 5C, proving the potential of MGv as a diagnostic marker for the differential diagnosis of OSCC. Additionally, the Youden index represented the best combination of specificity and sensitivity and was thus used as the optimum cut-off value. The Youden index was an MGv of 54, with a sensitivity of 93% and a specificity of 94%.

In Fig. 5A, the highlighted points marked as A1 and A2 represent the MGv measured near the threshold of 54 and SCC above the critical value in the healthy tissue.

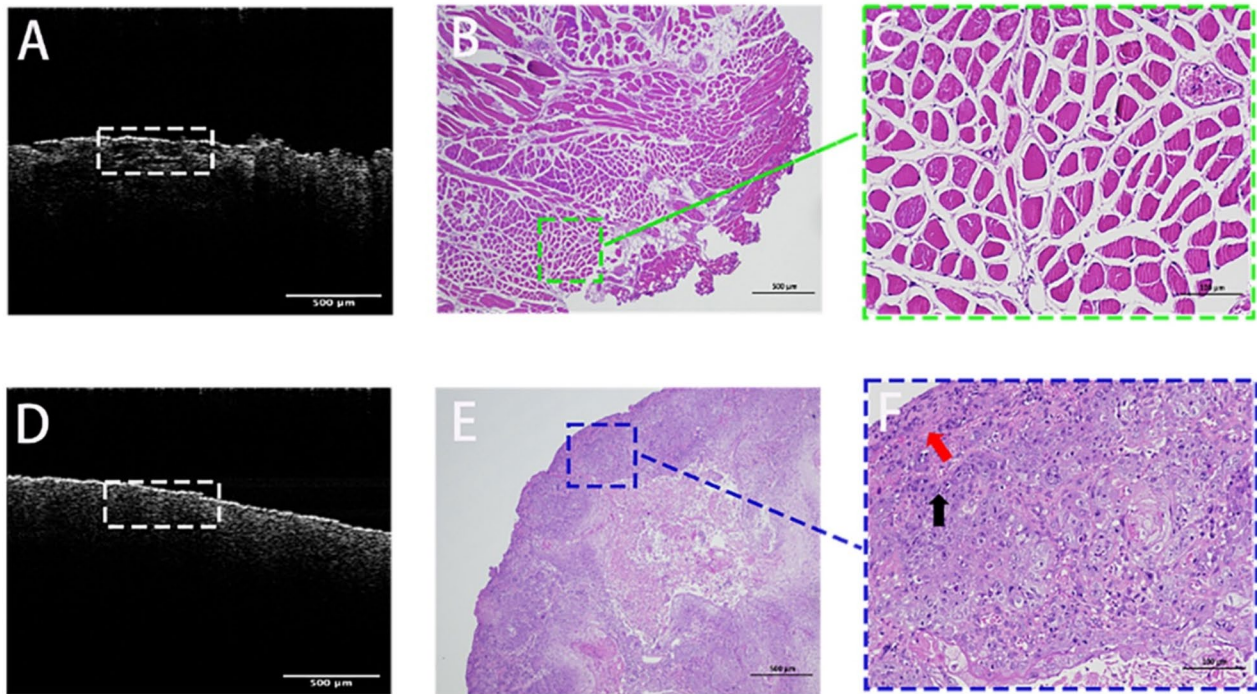


Fig. 4 Typical OCT and the corresponding histology: (A) OCT image of muscle tissue revealed tissue gaps (evident in the white box). (B) and (C) H&E staining revealed muscle tissue and fibres (40x and 200x), of normal morphology and structure, regular arrangement, and noticeable gaps. (D) OCT image of SCC; (E) and (F) H&E stained SCC sample (40x and 200x), a large number of tumour cells (black arrow) can be seen between the tissues, and connective tissue hyperplasia around the tumour tissue (red arrow). These images intend to demonstrate that OCT is capable of capturing images that closely correspond to a pathological reference standard, distinct from the method employed for MGV measurement within this experiment

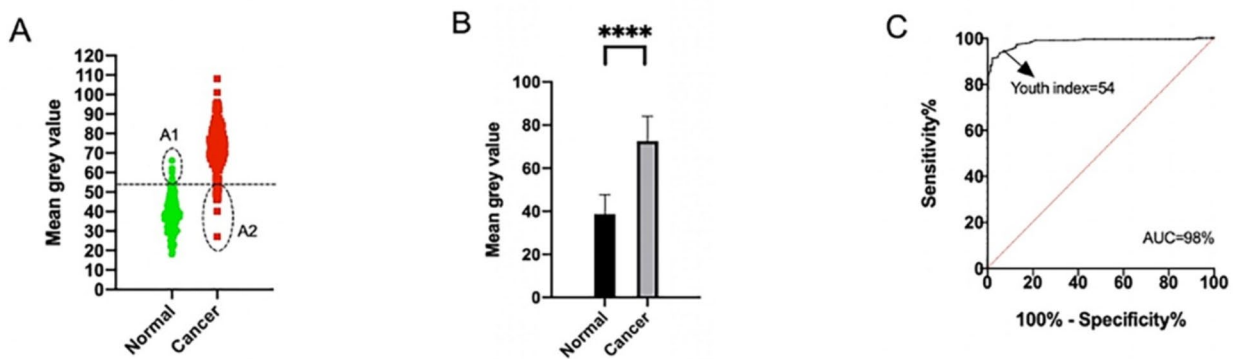


Fig. 5 MGV scatter plots (A), Mann-Whitney U test (B) for squamous cell carcinoma and normal tissue, and ROC curve (C) for distinguishing OSCC from normal tissue. (A) The green points represent the MGV measured in healthy tissue, and the red points represent the MGV measured in OSCC samples. The Youden index is shown as a dashed line and represents the cut-off value's position. (B) The Mann-Whitney U test calculated the p-value (< 0.0001). (C) The sensitivity and specificity were 0.93 and 0.94, respectively for the Youden index (when MGV was 54). The calculated area under the curve (AUC) was 0.98 and represented the discriminant ability

The nine measurements marked A1 in Fig. 5A were tissue locations consisting of a mixture of connective tissue and blood vessels, showing MGVs from 54.9 to 65.7. H&E staining of tissues at these locations revealed tightly structured tissues, which may have contributed to four MGV measurements that were above the 54 cut-off value but will need further investigation. SCC samples reported eleven MGVs around the cut-off value of 54, which also needs further evaluation to explain.

Discussion

Based on the OCT of para-cancerous tissues and information from related literature, the current study was designed to verify the possibility of discriminating tumours from surrounding (normal) tissues using MGVs. The data showed that the MGV differed between the tumour and normal tissues. Previously, differences in MGV were found in other tumours, such as the thyroid and breast. However, these studies were conducted using ultrasound and CT approaches [32, 33]. MGV in OCT was reported minimally, and the use of MGV assisted OCT to distinguish oral cancer from normal tissues was even rare.

Lv et al. reported that the grey value of malignant breast lesions was higher than that of benign lesions. In this study, a total of 299 lesions were used for calculation and comparison, including 101 benign lesions and 198 malignant lesions, and imaged by contrast-enhanced spectral mammography [32]. Han et al. further showed that the ultrasound grey scale ratio (UGSR) allowed the potential differentiation of papillary thyroid microcarcinomas (PTMCs) and micronodular goitres (MNGs).

UGSR is the ratio of grayscale value of lesions to that of the surrounding normal thyroid tissue. This novel method quantifies the echo intensity of thyroid lesions, whereby the stronger the echo intensity, the darker the black colouration and the higher the reading on the grey scale [33].

OCT is a non-invasive, real-time, and label-free tomography image generator for biological structures according to different optical properties between tissues. These properties help diagnose cancer early in both animals and humans and monitor tumour treatment, including SCC. Wilder et al. used OCT to diagnose SCC in golden Syrian hamster cheek pouches [34].

OCT imaging reports an 80% consistency with histopathology. Other experiments have also shown that OCT can effectively distinguish normal oral tissues from malignant lesions by detecting the change in tissue structure, including epithelial and keratin, identifying the basement membrane and the intensity of the OCT signal. For example, Hamdoon et al. used OCT to examine 125 suspicious oral lesions from 125 patients, with a specificity of 78% and a sensitivity of 85% [35]. Jerjes et al., using

the same method, had similar results, with 94.9% specificity and 83.3% sensitivity [36].

In studying the surgical margin of OSCC, Hamdoon et al. used OCT to determine the adequacy of immediate post-resection margins in OSCC, with a sensitivity of 81.5% and specificity of 87% [20]. In a following human study, Sumsum et al. used OCT to diagnose tumours and marginal zone malignant tumours with a sensitivity and specificity of 100%, which was equivalent to histological diagnosis [5]. Although encouraging, these results have not been translated into clinical application because of the lack of quantitative analysis and unified diagnostic criteria. This research aimed to provide a new quantitative indicator to discriminate tumours from surrounding tissues. We innovatively used MGV for quantitative analysis in OCT to assist in distinguishing squamous cell carcinoma tissue from normal tissue.

MGV is usually highly dependent on many factors, such as the selected region of interest, the size of the ROI, and the ROI's depth to the tissue's superficial surface. The major reason is that signal intensity weakens with the imaging depth, so if the ROI area is too large, it may include areas with attenuated signal intensity. Consequently, we established criteria for MGV measurement. On the one hand, the size of the regions of interest (ROI) in this experiment was the same (0.5 mm×0.1 mm). On the other hand, the imaging area of the ROI was positioned as superficially as possible, excluding any regions with a black background. The chosen depth was limited to 0.1 mm, thereby ensuring that the ROI remained within the zone of peak signal intensity in the OCT image and did not encompass areas of diminished signal.

There are several limitations to this study. Firstly, a better inference could be made if the sample size was bigger than the eighteen patients used in this study. With the increase in sample size, the presumption remains that measuring transition zones between the tumour and the surrounding healthy tissue helps explain the occurrence and development of the tumour, thus should be applied next and focused on the peri-tumour area. In addition, we will compare between cancerous squamous epithelium with mild, moderate, and severe dysplasia epithelium.

Secondly, The reason why the MGV of tumor tissue is higher than that of normal tissue is also what we need to study next. Thirdly, is that specific software is still needed to analyse MGV, which may limit the application of MGV in OCT images as a marker for detecting OSCC. This can be solved by developing OCT imaging software that can simultaneously analyse MGVs. Fourthly, we only studied tongue cancer and tongue tissue. We did not compare whether there were differences in MGV in different anatomic sites, nor did we compare whether there were differences in squamous cell carcinoma in

different anatomic sites. This is a future research direction. Moreover, a single quantitative index of MGV cannot ultimately assist OCT in differentiating normal oral tissues from tumour tissues, necessitating the exploration of more quantitative indexes for this purpose. Finally, at present, the current equipment cannot be used during an operation. However, the current data creates the possibility of building a device that can be used intraoperatively. Unlike the current detection that only covers selected measurement locations, the ultimate goal is to detect all resection margins.

Conclusion

In conclusion, the current experiment shows that the MGV of OSCC in OCT images is significantly higher than in surrounding healthy tissues. Therefore, MGV can help distinguish a tumour from its surrounding normal tissue. The MGV-specific information obtained in this study can be used to establish an *in vivo* OCT boundary demarcation method for OSCC. OCT is also a real-time imaging tomography used in head and neck surgeries consisting of a hand-held probe. This makes it possible to develop the application of *in vitro* and *in vivo* surgeries to assist and guide tumour surgery and achieve a sufficient range of successful resections.

Author contributions

Kangwei Zhou, Kaili Zheng and Li Huang made substantial contributions to the experiment and manuscript preparation. Xianglong Zheng, Canyang Jiang, Jianping Huang and Rihui Wang made substantial contributions to the data acquisition and preparation of the manuscript. Xin Ruan, Weicai Jiang and Wen Li have been involved in data analysis. Lisong Lin and Qingliang Zhao made substantial contributions to the conception and design of the study. All authors made manuscript reviews and approved the final manuscript for publication.

Funding

This study was supported by the Joint Funds for the Innovation of Science and Technology of Fujian province(2019Y9128).

Data availability

The datasets used and/or analysed during the current study available from the corresponding author on reasonable request.

Declarations

Competing interests

The authors declare no competing interests.

Ethics approval and consent to participate

The criteria and procedures for the inclusion of participants in this study were in accordance with the criteria indicated in the 1964 Helsinki Declaration. This study was approved by the Ethics Committee of The First Affiliated Hospital of Fujian Medical University (approval number:2019289).

Informed consent

Informed consent was obtained from all individual participants included in this study.

Received: 7 November 2023 / Accepted: 13 August 2024

Published online: 27 August 2024

References

- Sun L, Xu YR, Zhang XM, Gao Y, Chen JM, Zhou AW, Lu QB, Wang ZY, Shao KF, Wu HM, Ning XH. Mesenchymal stem cells functionalized sonodynamic treatment for improving therapeutic efficacy and compliance of orthotopic oral cancer. *Adv Mater*. 2020;32:e2005295. <https://doi.org/10.1002/adma.202005295>.
- Smits RW, Koljenović S, Hardillo JA, Ten Hove I, Meeuwis CA, Sewnaik A, Dronkers EA, Bakker Schut TC, Langeveld TP, Molenaar J, Hegt VN, Puppels GJ, de Baatburg RJ. Resection margins in oral cancer surgery: room for improvement. *Head Neck*. 2016;38:E2197–203. <https://doi.org/10.1002/hed.24075>.
- Dillon JK, Brown CB, McDonald TM, Ludwig DC, Clark PJ, Leroux BG, Futran ND. How does the close surgical margin impact recurrence and survival when treating oral squamous cell carcinoma? *J Oral Maxillofac Surg*. 2015;73:1182–8. <https://doi.org/10.1016/j.joms.2014.12.014>.
- Ferlay J, Soerjomataram I, Dikshit R, Eser S, Mathers C, Rebelo M, Parkin DM, Forman D, Bray F. Cancer incidence and mortality worldwide: sources, methods and major patterns in GLOBOCAN 2012. *Int J Cancer*. 2015;136:E359–86. <https://doi.org/10.1002/ijc.29210>.
- Sunny SP, Agarwal S, James BL, Heidari E, Muralidharan A, Yadav V, Pillai V, Shetty V, Chen Z, Hedne N, Wilder-Smith P, Suresh A, Kuriakose MA. Intraoperative point-of-procedure delineation of oral cancer margins using optical coherence tomography. *Oral Oncol*. 2019;92:12–9. <https://doi.org/10.1016/j.oraloncology.2019.03.006>.
- Kain JJ, Birkeland AC, Udayakumar N, Morlandt AB, Stevens TM, Carroll WR, Rosenthal EL, Warram JM. Surgical margins in oral cavity squamous cell carcinoma: current practices and future directions. *Laryngoscope*. 2020;130:128–38. <https://doi.org/10.1002/lary.27943>.
- Varvares MA, Poti S, Kenyon B, Christopher K, Walker RJ. Surgical margins and primary site resection in achieving local control in oral cancer resections. *Laryngoscope*. 2015;125:2298–307. <https://doi.org/10.1002/lary.25397>.
- KleinJan GH, van Werkhoven E, van den Berg NS, Karakullukcu MB, Zijlman HJMAA, van der Hage JA, van de Wiel BA, Buckle T, Klop WMC, Horenblas S, Valdés Olmos RA, van der Poel HG, van Leeuwen FWB. The best of both worlds: a hybrid approach for optimal pre- and intraoperative identification of sentinel lymph nodes. *Eur J Nucl Med Mol Imaging*. 2018;45:1915–25. <https://doi.org/10.1007/s00259-018-4028-x>.
- Yahalom R, Dobriyan A, Vered M, Talmi YP, Teicher S, Bedrin L. A prospective study of surgical margin status in oral squamous cell carcinoma; a preliminary report. *J Surg Oncol*. 2008;98:572–8. <https://doi.org/10.1002/jso.21034>.
- Pires L, Demidov V, Wilson BC, Salvio AG, Moriyama L, Bagnato VS, Vitkin IA, Kurachi C. Dual-agent photodynamic therapy with optical clearing eradicates pigmented melanoma in preclinical tumor models. *Cancers (Basel)*. 2020;12:1–17. <https://doi.org/10.3390/cancers12071956>.
- Roblyer D, Kurachi C, Stepanek V, Williams MD, El-Naggari AK, Lee JJ, Gil-enwater AM. Objective detection and delineation of oral neoplasia using autofluorescence imaging. *Cancer Prev Res*. 2009;2:423–31. <https://doi.org/10.1158/1940-6207.CAPR-08-0229>.
- Jeng MJ, Sharma M, Sharma L, Chao TY, Huang SF, Chang LB, Wu SL, Chow L. Raman Spectroscopy Analysis for Optical diagnosis of oral Cancer detection. *J Clin Med*. 2019;8:1313. <https://doi.org/10.3390/jcm8091313>.
- Barroso EM, Ten Hove I, Bakker Schut TC, Mast H, van Lanschot CGF, Smits RWH, Caspers PJ, Verdijk R, Noordhoek Hegt V, Baatburg de Jong RJ, Wolvius EB, Puppels GJ, Koljenović S. Raman spectroscopy for assessment of bone resection margins in mandibulectomy for oral cavity squamous cell carcinoma. *Eur J Cancer*. 2018;92:77–87. <https://doi.org/10.1016/j.ejca.2018.01.068>.
- Buckley H, Wilson C, Ajithkumar T. High-dose-rate brachytherapy in the management of operable rectal cancer: a systematic review. *Int J Radiat Oncol Biol Phys*. 2017;99:111–27. <https://doi.org/10.1016/j.ijrobp.2017.05.023>.
- Chen PH, Lee HY, Chen YF, Yeh YC, Chang KW, Hou MC, Kuo WC. Detection of oral dysplastic and early cancerous lesions by polarization-sensitive optical coherence tomography. *Cancers (Basel)*. 2020;12:1–18. <https://doi.org/10.3390/CANCERS12092376>.
- Zhao T, Huang G, Li Y, Yang S, Ramezani S, Lin Z, Wang Y, Ma X, Zeng Z, Luo M, de Boer E, Xie XJ, Thibodeaux J, Brekken RA, Sun X, Sumer BD, Gao J. A transistor-like pH Nanoprobe for Tumour Detection and Image-guided surgery. *Nat Biomed Eng*. 2016;1. <https://doi.org/10.1038/S41551-016-0006>.
- Barroso EM, Smits RW, van Lanschot CG, Caspers PJ, Ten Hove I, Mast H, Sewnaik A, Hardillo JA, Meeuwis CA, Verdijk R, Noordhoek Hegt V, Baatburg de Jong RJ, Wolvius EB, Bakker Schut TC, Koljenović S, Puppels GJ. Water concentration analysis by Raman spectroscopy to determine the location of the

- tumor border in oral cancer surgery. *Cancer Res.* 2016;76:5945–53. <https://doi.org/10.1158/0008-5472.can-16-1227>.
18. Shin D, Vigneswaran N, Gillenwater A, Richards-Kortum R. Advances in fluorescence imaging techniques to detect oral cancer and its precursors. *Futur Oncol.* 2010;6:1143–54. <https://doi.org/10.2217/fon.10.79>.
 19. Tirelli G, Piovesana M, Gatto A, Tofanelli M, Biasotto M, Boscolo Nata F. Narrow band imaging in the intra-operative definition of resection margins in oral cavity and oropharyngeal cancer. *Oral Oncol.* 2015;51:908–13. <https://doi.org/10.1016/j.oraloncology.2015.07.005>.
 20. Hamdoon Z, Jerjes W, McKenzie G, Jay A, Hopper C. Optical coherence tomography in the assessment of oral squamous cell carcinoma resection margins. *Photodiagnosis Photodyn Ther.* 2016;13:211–7. <https://doi.org/10.1016/j.pdpdt.2015.07.170>.
 21. Matsui Y, Kondo M, Uchiyama E, Miyata R, Matsubara H. New clinical ultrahigh-resolution SD-OCT using A-scan matching algorithm. *Graefes Arch Clin Exp Ophthalmol.* 2019;257:255–63. <https://doi.org/10.1007/s00417-018-4183-6>.
 22. Arcadi F, Benmansour F, Maunz A, Michon J, Haskova Z, McClintock D, Adamis AP, Willis JR, Prunotto M. Deep learning predicts OCT measures of diabetic macular thickening from color fundus photographs. *Investig Ophthalmol Vis Sci.* 2019;60:852–7. <https://doi.org/10.1167/iovs.18-25634>.
 23. Huynh E, Chandrasekera E, Bukowska D, McLenachan S, Mackey DA, Chen FK. Past, present, and future concepts of the choroidal scleral interface morphology on optical coherence tomography. *Asia-Pacific J Ophthalmol.* 2017;6:94–103. <https://doi.org/10.22608/apo.201698>.
 24. Huang D, Swanson EA, Lin CP, Schuman JS, Stinson WG, Chang W, Hee MR, Flotte T, Gregory K, Puliafito CA. Optical coherence tomography. *Science.* 1991;254:1178–81. <https://doi.org/10.1126/science.1957169>.
 25. Yang Z, Shang J, Liu C, Zhang J, Liang Y. (2022) Identification of oral precancerous and cancerous tissue by swept source optical coherence tomography. [J]. *Lasers Surg Med.* 2022, 54: 320–328. <https://doi.org/10.1002/lsm.23461>
 26. Lee CU, Chong S, Choi HW, Choi JC. Quantitative image analysis using chest computed tomography in the evaluation of lymph node involvement in pulmonary sarcoidosis and tuberculosis. *PLoS ONE.* 2018;13:e0207959. <https://doi.org/10.1371/journal.pone.0207959>.
 27. Rai H, Hussein H, Collieran R, Xhepa E, Wiebe J, Piniack S, Cassese S, Joner M, Kastrati A, Byrne RA, Foley DP. Optical coherence tomography tissue coverage and characterization with grey-scale signal intensity analysis after bifurcation stenting with a new generation bioabsorbable polymer drug-eluting stent. *Cardiovasc Revascularization Med.* 2020;21:277–85. <https://doi.org/10.1016/j.carrev.2019.05.004>.
 28. AlMadi DM, Al-Hadlaq MA, AlOtaibi O, Alshagroud RS, Al-Ekrish AA. Accuracy of mean grey density values obtained with small field of view cone beam computed tomography in differentiation between periapical cystic and solid lesions. *Int Endod J.* 2020;53:1318–26. <https://doi.org/10.1111/iej.13355>.
 29. Huang D, Wang G, Mao J, Liu C, Fan Z, Zhang Y, Zhang B, Zhao Y, Dai C, He Y, Ma H, Liu G, Chen X, Zhao Q. Intravital whole-process monitoring Thermo-Chemotherapy Via 2D Silicon Nanoplatfrom: a Macro Guidance and Long-Term Microscopic Precise Imaging Strategy. *Adv Sci (Weinh).* 2021;2021(8):e2101242. <https://doi.org/10.1002/adv.202101242>.
 30. Huang Y, Li M, Huang D, Qiu Q, Lin W, Liu J, Yang W, Yao Y, Yan G, Qu N, Tuchin VV, Fan S, Liu G, Zhao Q, Chen X. Depth-resolved enhanced spectral-domain OCT imaging of live mammalian embryos using gold nanoparticles as contrast Agent. *Small.* 2019;2019(15):e1902346. <https://doi.org/10.1002/smll.201902346>.
 31. Zhao Q, Dai C, Fan S, Lv J, Nie L. Synergistic efficacy of salicylic acid with a penetration enhancer on human skin monitored by OCT and diffuse reflectance spectroscopy. *Sci Rep.* 2016;2016(6):34954. <https://doi.org/10.1038/srep34954>.
 32. Lv Y, Chi X, Sun B, Lin S, Xing D. Diagnostic Value of Quantitative Gray-Scale Analysis of Contrast-Enhanced Spectral Mammography for Benign and malignant breast lesions. *J Comput Assist Tomogr.* 2020;44:405–12. <https://doi.org/10.1097/rct.0000000000001019>.
 33. Han Z, Lei Z, Li M, Luo D, Ding J. Differential diagnosis value of the ultrasound gray scale ratio for papillary thyroid microcarcinomas and micronodular goiters. *Quant Imaging Med Surg.* 2018;8:507–13. <https://doi.org/10.21037/qims.2018.06.04>.
 34. Wilder-Smith P, Jung WG, Brenner M, Osann K, Beydoun H, Messadi D, Chen Z. In vivo optical coherence tomography for the diagnosis of oral malignancy. *Lasers Surg Med.* 2004;35:269–75. <https://doi.org/10.1002/lsm.20098>.
 35. Hamdoon Z, Jerjes W, Upile T, McKenzie G, Jay A, Hopper C. Optical coherence tomography in the assessment of suspicious oral lesions: an immediate ex vivo study. *Photodiagnosis Photodyn Ther.* 2013;10:17–27. <https://doi.org/10.1016/j.pdpdt.2012.07.005>.
 36. Jerjes W, Hamdoon Z, Al Rawi N, Hopper C. OCT in the diagnosis of head and neck pre-cancerous and cancerous cutaneous lesions: an immediate ex vivo study. *Photodiagnosis Photodyn Ther.* 2019;27:481–6. <https://doi.org/10.1016/j.pdpdt.2019.07.019>.

Publisher's note

Springer Nature remains neutral with regard to jurisdictional claims in published maps and institutional affiliations.